

APPROVED FOR PUBLIC RELEASE
DISTRIBUTION UNLIMITED

ADA076 054

WADC TECHNICAL REPORT 52-88

INTERIM REPORT ON A STUDY OF MACH ONE WIND TUNNELS

**DAVID T. BARISH, CAPT, USAF
AIRCRAFT LABORATORY**

APRIL 1952

**Reproduced From
Best Available Copy**

WRIGHT AIR DEVELOPMENT CENTER

20020104151

NOTICES

When Government drawings, specifications, or other data are used for any purpose other than in connection with a definitely related Government procurement operation, the United States Government thereby incurs no responsibility nor any obligation whatsoever; and the fact that the Government may have formulated, furnished, or in any way supplied the said drawings, specifications, or other data, is not to be regarded by implication or otherwise as in any manner licensing the holder or any other person or corporation, or conveying any rights or permission to manufacture, use, or sell any patented invention that may in any way be related thereto.

The information furnished herewith is made available for study upon the understanding that the Government's proprietary interests in and relating thereto shall not be impaired. It is desired that the Judge Advocate (WCJ), Wright Air Development Center, Wright-Patterson Air Force Base, Ohio, be promptly notified of any apparent conflict between the Government's proprietary interests and those of others.

////////////////////

This document contains information affecting the National defense of the United States within the meaning of the Espionage Laws, Title 18, U.S.C., Sections 793 and 794. Its transmission or the revelation of its contents in any manner to an unauthorized person is prohibited by law.

INTERIM REPORT ON A STUDY OF MACH ONE WIND TUNNELS

*David T. Barish, Capt, USAF
Aircraft Laboratory*

April 1952

RDO No. 458-429

Wright Air Development Center
Air Research and Development Command
United States Air Force
Wright-Patterson Air Force Base, Ohio

FOREWORD

This report was prepared by the Wind Tunnel Branch, Aircraft Laboratory, Wright Air Development Center, under Research and Development Order Number 458-429, "Dimensional and Axially Symmetric Transonic Flow."

The author wishes to express his gratitude to Dr. K. G. Guderley for contributing the leading theoretical ideas behind this study, and also for his continued encouragement and guidance.

This work was performed while the author was assigned as project engineer, Theoretical Aerodynamics Unit, in the Wind Tunnel Branch, WADC.

ABSTRACT

The simulation in wind tunnels of flows with a sonic free stream velocity is studied from the theoretical standpoint, and a preliminary experimental phase is also described.

The solutions which are valid asymptotically are extended to include higher order terms so that flow patterns at distances of technical interest from bodies with and without lift can be discussed. This is done with a view toward determining the essential characteristics which streamlines near a wind tunnel wall would have to possess if the simulation of Mach One flow were to be obtained, and also toward determining which body shape parameters are needed in order to apply the correct scale factors. The results indicate that the ratio of model to tunnel size where a single parameter is sufficient to give the conditions at the wall is quite large.

A set of preliminary wind tunnel tests was made with inclined plane walls in the test section. This approximation of the correct streamline contour yielded data which appears to be in good agreement with the theoretical results at Mach One.

The security classification of the title of this report is UNCLASSIFIED.

PUBLICATION REVIEW

This report has been reviewed and approved.

FOR THE COMMANDING GENERAL:



R. G. RUEGG
Colonel, USAF
Chief, Aircraft Laboratory
Aeronautics Division

TABLE OF CONTENTS

| <u>Section</u> | <u>Page</u> |
|---|-------------|
| I Analytical Study | 1 |
| Formulation of the Problem | 1 |
| Streamline Shapes | 2 |
| Cusped Body | 3 |
| Wedge Profile | 4 |
| Comparison of the Two Bodies | 5 |
| Asymptotic Solutions in the Physical Plane | 5 |
| Similarity Considerations | 6 |
| Correlation of Basic Planar Solutions in the Physical Plane with Hodograph Solutions | 7 |
| Lifting Cases | 9 |
| Cusped Lifting Bodies | 9 |
| Wedge Profile with Lift | 10 |
| II Preliminary Experimental Study | 11 |
| Experimental Equipment | 12 |
| 1. Wind Tunnel | 12 |
| 2. Optical Equipment | 12 |
| 3. Wedge Model (See Figure 10) | 12 |
| 4. Biconvex Model (See Figure 12) | 13 |
| Wind Tunnel Runs | 13 |
| Discussion of Experimental Results | 13 |
| Wedge at Angle of Attack | 14 |
| Biconvex Section | 15 |
| Conclusions | 15 |
| References | 17 |

LIST OF ILLUSTRATIONS

| Figure | | Page |
|--------|--|------|
| 1. | Theoretical Data for Cusped Body. | 18 |
| 2. | Theoretical Data for Wedge Profiles. | 19 |
| 3. | Asymptotic Solutions in the Physical Plane. | 20 |
| 4. | Theoretical Data for Cusped Body with Lift. | 21 |
| 5. | Comparison of Experimental and Theoretical Data for Wedge at Station 46. | 22 |
| 6. | Experimental Wall Pressure Distributions for Tranverses of 20° Wedge. | 23 |
| 7. | Experimental Wall Pressures for 20° Wedge with Lift (Upper Wall). | 24 |
| 8. | Experimental Data for 20° Wedge at Station 46. | 25 |
| 9. | Schlieren Photographs of Model Tranverses. | 26 |
| 10. | Wedge Model. | 27 |
| 11. | Experimental Pressure Distribution for Biconvex Section. | 28 |
| 12. | Interferogram of Biconvex Model. | 29 |

LIST OF SYMBOLS

- a velocity of sound
- a_0 stagnation velocity of sound
- A_N coefficient of potential
- C_p pressure coefficient = $(p-p^*)/q^*$
- C_L lift coefficient
- γ ratio of specific heats
- P static pressure
- q dynamic pressure
- W velocity modulus
- X,Y cartesian coordinates
- x_0, y_0 coordinates of body at sonic point
- \bar{y} streamline deviational ordinate
- Z_1 similarity parameter
- Z_2 scale factor
- α angle of attack
- $\eta = (\gamma + 1)^{\frac{1}{3}} \left(\frac{W}{W^*} - 1 \right)$
- θ inclination of velocity vector
- $\xi = 9\theta^2/4\eta^3$
- ξ similarity parameter in physical plane
- ρ density
- ϕ velocity potential
- ψ stream function
- Ω perturbation potential
- * conditions where velocity is sonic
- o fixed value to be defined

INTRODUCTION

In recent years the interest in obtaining data for models operating in the immediate vicinity of the sonic velocity has been quite persistent. Such quantities as local Mach number distribution and drag have been shown to have a smooth behavior as Mach One is passed, but it is not clear how the values of the lift curve slopes, inter-action coefficients, duct efficiencies, stability derivatives, and other characteristics which are sensitive to the relative sizes of the subsonic and supersonic regions behave in mixed flows.

Present methods utilizing free flight models, transonic bumps, and very small models in large wind tunnels have provided some excellent qualitative data, but there does not seem to be an experimental technique which can provide the degree of accuracy normally obtainable from wind tunnels operating outside the transonic range. However, there are several techniques currently under consideration for filling this gap.

The purpose of the present investigation is to study the extent to which wind tunnels can be used to determine the aerodynamic characteristics of models in the immediate vicinity of Mach One.

The approach used is to first consider the distortion of the tunnel walls which would be necessary in order to simulate a streamline in a free flow field. In the type of theoretical analysis used it is possible to express the velocity potential as a "basic" potential plus a series of higher order particular potentials which are added to satisfy the boundary conditions at the body. The basic potential is the one which is significant at large distances from the body, and therefore largely determines the wall configuration.

To obtain a general feeling for the actual effect of higher order terms due to the shape and lift of bodies on the flow fields at various distances from a particular model, these data have been computed for several simple bodies and the results are compared with the solutions given by the basic potential alone.

The distances from the bodies where the influence of the higher order terms become of the same general proportions as the experimental scatter gives a fairly good indication of the ratio of model to tunnel size where the influence of the tunnel wall on any model of a certain group would not be significant in the results.

This report, which represents the first part of a larger program, gives an account of the analytical study, and in addition, the results of a preliminary experimental program. In the experimental phase, the ideal wall shape was approximated by a nozzle block with a throat followed by a long straight section set at an angle. A comparison of these results with the analytical data seems to be quite encouraging despite the approximation used.

SECTION I

ANALYTICAL STUDY

It is somewhat more convenient to treat the case of planar flow first, since the hodograph differential equations are linear. The general approach is that used by Dr. K. G. Guderley (Reference 1).

Formulation of the Problem

The differential equation for the velocity potential, ϕ , can be simplified in the case of small perturbations of a flow with sonic free stream velocity to:

$$(\gamma+1)\phi_x \phi_{xx} - \phi_{yy} = 0 \quad (1)$$

With the introduction of the inclination of the velocity vector θ , and the dimensionless perturbation velocity given by $\eta = (\gamma+1)^{\frac{1}{2}} (\frac{w}{w_\infty} - 1)$ as variables, the application of the Legendre transformation yields in the hodograph plane, the Tricomi equation: $\phi_{\eta\eta} - \eta\phi_{\theta\theta} = 0$ (2)

A set of solutions to this is given by:

$$\phi = -\alpha_0 w^4 (\gamma+1)^{-\frac{1}{2}} \left[A_{-1} \eta^{-1} f_{-1}(\xi) + \sum_{n=1}^M \eta^n f_n(\xi) \right] \quad (3)$$

where $n = m/2$ and $\xi = 9\theta^2/4\eta^3$. The functions $f_n(\xi)$ satisfy the

$$\text{equation: } f_n'' \xi(\xi-1) + f_n' \left[\left(\frac{4}{3} - \frac{2n}{3} \right) \xi - \frac{1}{2} \right] + \frac{n(n-1)}{9} f_n = 0$$

It is the hypergeometric function, f_1 , used in Reference 1. The values of the coefficients A_n are to be determined.

Working with these functions reveals that the even values of m give various symmetrical body shapes. The addition of odd values gives asymmetrical bodies.

The corresponding points in the physical plane are given by:

$$\begin{aligned} x &= \frac{\partial \phi}{\partial \eta} \frac{1}{\alpha_0 w^4} \left[A_{-1} |\eta|^{-2} (f_{-1} + 3\xi f_{-1}') + \sum_{n=1}^M A_n |\eta|^{n-1} (-n f_n + 3\xi f_n') \right] \text{sign } \eta \\ y &= \frac{\partial \phi}{\partial \theta} \frac{(\gamma+1)^{-\frac{1}{2}}}{\alpha_0 w^4} = -3(\gamma+1)^{-\frac{1}{2}} |\xi|^{\frac{1}{2}} \left[A_{-1} |\eta|^{-\frac{5}{2}} f_{-1}' + \sum_{n=1}^M A_n |\eta|^{n-\frac{3}{2}} f_n' \right] \text{sign}(\eta\theta) \end{aligned} \quad (4)$$

By using the consistent approximation that $y = 0$ at the body, it is possible with these expressions to prescribe the values of x and y at M points on a given body from a resultant system of $(M + 1)$ equations in $(M + 1)$ unknowns and hence, to find the values of $\Delta\eta$ and η . The position of the nose of the body is given by the branch point of the streamlines in the hodograph plane. This occurs at a finite value of $|\eta|$; i.e., there is no stagnation point. Therefore, all such bodies have cusped leading edges.

It should be mentioned that the $(M + 1)$ expressions are non-linear and furthermore the question is not settled as to whether the procedure converges as M is increased. Consequently it is possible that the points at the boundary where matching does not occur will oscillate in an undesirable manner.

Streamline Shapes

The vertical deviation of a streamline from its original position far upstream is given by $\tilde{Y} = \int_{-\infty}^{x_0} \phi_Y dx$. The zero subscript denotes the space point considered. Because of the differential equation (1), the following expression can be written:

$$\iint_S [\phi_X \phi_{XX} (\gamma + 1) - \phi_{YY}] dx dY = 0$$

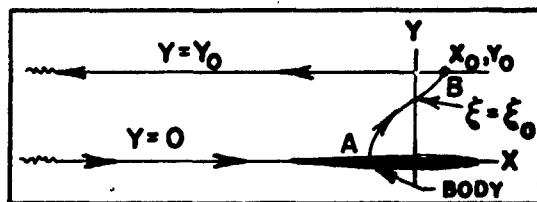
Using Green's theorem one obtains

$$\int_C (\gamma + 1) \frac{\phi_X^2}{2} dY + \int_C \phi_Y dx = 0$$

If a closed contour is chosen which is given by the lines $Y=0, Y=Y_0, X=-\infty$,

(See Sketch)

and the line AB which arises from the mapping of a line $\xi = \xi_0$ from the hodograph to the physical plane.



All terms drop out except:

$$\int_{-\infty}^{x_0} [\phi_Y]_{Y=Y_0} dx = \int_0^{Y_0} \left[(\gamma + 1) \frac{\phi_X^2}{2} + \phi_Y \frac{dx}{dY} \right]_{\xi=\xi_0} dY + \int_{-\infty}^{\xi_0} [\phi_Y]_{Y=0} dx$$

The integral on the left gives the streamline displacement at $Y=Y_0$, $\xi=\xi_0$

If we transpose to the hodograph and integrate

$$\bar{Y}-\bar{Y}_0 = \left| \xi_0 \right|^{\frac{1}{2}} \sum_{n=0}^M A_n \left[\frac{\eta^{n+\frac{1}{2}}}{\eta+\frac{1}{2}} \right] \eta \left[\frac{3}{2}(n+\frac{3}{2}) + \frac{2}{3}(n-1)(-nf'_n + 3\xi f'_n) \right] \quad (5)$$

where $\eta_0(\xi_0)$ is the value of η for $Y=0$ and where \bar{Y}_0 is the displacement of the streamline $\psi = 0$. In symmetrical flows, Y_0 gives the actual body shape. It can readily be obtained by the summation of $\theta \Delta x$ from the nose to the value of ξ_0 considered.

Cusped Body

The simplest body which has been investigated by this method is given by the potentials for $n = -1$ and $n = 2$. This is a cusped profile with a constant pressure gradient over its length. For such a body, the transformed velocity potential is given by

$$\phi = (\gamma+1)^{-\frac{1}{3}} a_0 w^* \left[A_1 \eta^{\frac{1}{2}} f_1 + A_2 \eta^{\frac{3}{2}} f_2 \right] \quad (6)$$

and the stream function by: (see page 27, Reference 1)

$$\psi = -a_0 w^* (\gamma+1)^{-\frac{1}{3}} \frac{1}{3\rho^* |\xi|^{1/2}} \text{SIGN}(\eta\theta) \left[A_1 |\eta|^{\frac{5}{2}} f_1' + A_2 |\eta|^{\frac{7}{2}} f_2' \right] \quad (7)$$

Along the body, $\psi = 0$ and equation (7) gives

$$\eta_0 = - \left| \frac{A_1 f_1'}{A_2 f_2'} \right|^{1/3} \quad (8)$$

Substitution into (4) yields $x_0 = A_2 \eta_0$. Using equation (4), (5), and (8) the pressure fields, deviational ordinates, and body profiles were computed for $A_2/A_1 = 10, 100$ and $1,000$. These patterns were compared with the patterns given by "basic" potential ($n = -1$), and the results $A_2/A_1 = 100$ are shown in Figure 1. It can be seen from the comparison curves of this figure that if ± 0.1 is chosen arbitrarily as the experimental scatter in C_p , if ($\gamma = 1.4$), and if $\gamma > 800 A_1$, the differences between the two curves will be of the order of the scatter.

If x_0 is the length of a body from the nose to the sonic point on the body, and y_0 , the body ordinate at that point, and if the value of A_1 is fixed, the bodies which arise from various values of A_2 all have

the same value of y_0^4/x_0 . Accordingly, there exists a "bluntness factor"; i.e., blunt bodies which have a smaller actual thickness can influence the asymptotic solution to the same extent as a thicker body with

a higher slenderness ratio. It will be shown later that, y_0^4/x_0 ,

is a characteristic parameter which will be the same for all affine bodies which have the same asymptotic flow fields.

Wedge Profile

Guderley and Yoshihara have computed the pressures on a wedge at Mach One for both the symmetrical (Reference 2) and asymmetrical (Reference 5) cases. It is a fairly straightforward procedure to find the flow field in the vicinity of such a body as follows: There are three convenient forms of solutions in addition to the set of solutions mentioned in the previous section. They are:

$$\phi_1 = -A_{-1} |\eta|^{-1} \sum_{m=-\infty}^{\infty} f_{-1}(\zeta_m) \quad \zeta_m = 9(\theta - 2m\theta)^2 / 4\eta^{3/2} \quad (9)$$

$$\phi_2 = \sum_{m=0}^{\infty} A_{2m+1} \frac{g(\eta, 2m+1)}{g(\frac{3}{4}\theta_0, 2m+1)} \cos(2m+1) \frac{\theta}{\theta_0} \quad (10)$$

$$\phi_3 = -\frac{\theta_0}{\pi} \sum_{m=0}^{\infty} \frac{b_m}{m} \frac{g(\eta, m)}{g(\frac{3}{4}\theta_0, m)} \cos m\pi \frac{\theta}{\theta_0} \quad (11)$$

where f_{-1} is the same hypergeometric function discussed previously and in this case represents singularities spaced along the line $\eta = 0$ at

intervals of $2\theta_0$. $\phi = \phi_1 + \phi_2 + \phi_3$ satisfies the boundary condition $\psi = 0$ at $\theta = \pm\theta_0$, the semi-angle of the wedge. In ϕ_2 and ϕ_3 , the function $g(\eta, m)$ is given by $g(\eta, m) = |\eta|^{1/2} Z_{\frac{1}{3}}(\frac{2m\pi\eta^{3/2}}{3\theta_0})$ where $Z_{\frac{1}{3}}$ is a linear combination of Bessel functions of order $1/3$.

These two solutions ϕ_2 and ϕ_3 are used to satisfy the boundary conditions along the characteristic in the supersonic region which emanates from the point $\eta = 0, \theta = \theta_0$.

Again, the predominant term near the origin of the plane is $f_{-1}(m=0)$ and one can find the influence of the other terms for various values of η , and θ .

This too was carried out for small values of η and θ . The resultant flow fields are shown in Figure 2a.

Comparison of the Two Bodies

It is of interest to compare these two bodies whose solutions now have been derived.

It θ_0 is the ratio Y_0/X_0 , the following table gives the numerical values which have been obtained for the cusped body and the wedge:

| | | |
|-------------------------|--------|-------|
| $X_0(\theta_0)^{4/3-1}$ | Cusped | Wedge |
| $A-1$ | 2.62 | 2.80 |
| $Y_0/X_0 A^{3/2-1}$ | 17.95 | 22.00 |

These values would be identical if the ratio of the values of the coefficients is given by $A_{-1c}/A_{-1w} = 1.070$. If this were true, for the cusped body $X_0 = 2.83 \theta_0^{-4/3}$ and for the wedge, $X_0 = 2.80 \theta_0^{-4/3}$.

These values are quite close and in light of the fact that the accuracy of the numerical methods used was about $\pm 1\%$, it can be said that within this accuracy, a wedge and cusped body which have the same lengths and heights to the sonic lines have the same effect on the asymptotic flow field. If this could be shown to be the general case, the problem of simulating Mach One flows would be greatly simplified.

Asymptotic Solutions in the Physical Plane

A method which was first used in Reference 3 is quite convenient for considering the asymptotic flow fields for both the planar symmetric and axisymmetric cases. The general technique has been used in Reference 4 to obtain the asymptotic shock wave patterns at Mach One.

With a free stream of sonic velocity, the velocity perturbation potential differential equation in the physical plane can be written as:

$$(\gamma + 1) \phi_x \phi_{xx} - \phi_{yy} - A \phi_{y/y} = 0 \quad (13)$$

In the planar case $A = 0$ and in the axisymmetric case $A = 1$. If a solution is assumed of the form $\phi = y^{3n-2} f(\xi)$ where $\xi = (\gamma + 1)^{1/3} xy^{-n}$ the resultant equation is $f''(n^2 \xi^2 - f') - n \xi f'(5n-5+A) - f(3n-2)(3n-3+A) = 0$

It has been determined that for the planar case $n = 4/5$ and for the axisymmetric case $n = 4/7$ (f is found by numerical integration). Asymptotically the shock coincides with a line of constant ξ . In the planar case $\xi = 2.018$, and in the axisymmetric case, $\xi = 2.240$. The streamline deviational ordinates are in the axisymmetric case given by:

$$\bar{y} = \frac{9}{2} y^{-5/7} \left[\frac{f'^2}{2} - \frac{8}{49} (f + 2\xi f') \right] = \frac{9}{2} y^{-5/7} \bar{y} \quad (14)$$

and in the planar case

$$\bar{y} = 5 y^{1/5} \left[\frac{f'^2}{2} - \frac{8}{25} \xi (f - 2\xi f') \right] = 5 y^{1/5} \bar{y} \quad (15)$$

Since it is simpler to obtain the flow field at a given value of x and y by this method, it was used extensively in this study. The plots of these functions are shown in Figure 1.

Similarity Considerations

If two separate systems are related by the following transformation:

$$\phi(x, y) = z_1 z_2 \bar{\phi}(\bar{x}, \bar{y}), \quad x = z_2 \bar{x}, \quad y = z_2 z_1^{-1/2} \bar{y} \quad (16)$$

Equation (13) becomes

$$(\gamma+1) \bar{\phi}_{\bar{x}} \bar{\phi}_{\bar{x}\bar{x}} - \bar{\phi}_{\bar{y}\bar{y}} - A \bar{\phi}_{\bar{y}} / \bar{y} = 0$$

The points in the two systems given by these relations are called "corresponding" points.

The preservation of the form of the differential equation indicates that if $\bar{\phi}$ is a solution for a flow problem in the \bar{x}, \bar{y} plane, then ϕ is a solution in the x, y plane. If $z_2 \neq 1, z_1 = 1$, only the scales of the two systems are different, and if $z_2 = 1, z_1 \neq 1$, The relations given above are known as the transonic similarity relations.

Consider the case where two different affine bodies in these two flow fields are producing the same conditions asymptotically; i.e., if the axes of the two systems were made to coincide, the velocities at a given point at a large distance would also coincide. Then the two flows are described asymptotically by the identical forms $\phi = Y^{3\gamma-2} f(\xi)$ and

$$\bar{\phi} = \bar{Y}^{3\gamma-2} f(\bar{\xi}). \quad \text{This may happen although } z_1 \text{ and } z_2 \text{ are not equal}$$

to one, but for the prescribed similarity to exist the values of ϕ and $\bar{\phi}$ must coincide at the identical point in space. In general the "identical" points will not be the "corresponding" points.

Using Equation 16 and the asymptotic expression for ϕ , the following is obtained: $\phi = z_1 z_2 (z_2 z_1^{-1/2})^{-(3\gamma-2)} Y^{3\gamma-2} f\left(\frac{x}{z_2} \left(\frac{y}{z_2 z_1^{-1/2}}\right)^{-\gamma}\right)$

If $z_2 = z_1^{1/(1-\gamma)}$ the expression reduces to $\phi = Y^{3\gamma-2} f(x Y^{-\gamma})$ independent of the value of z_1 or z_2 . Hence, with this relation between z_1 and z_2 , the values of ϕ and $\bar{\phi}$ and also ξ and $\bar{\xi}$ coincide at the identical points.

Now consider the possibility of relating the dimensions of two bodies which give asymptotically the same flows at identical points. If corres-

the above relation between Z_1 and Z_2 , $\overline{Y_1} = \overline{Y_1} Z_1^{\frac{4n-3}{2(1-n)}}$

This equation is independent of Z_1 if $\beta = -n/(4n-3)$. This value of

It is possible to go further and to say that if the values of x and \bar{x} at one set of corresponding points are denoted by the subscript 1 and the values of \tilde{y} and $\bar{\tilde{y}}$ are taken at another set denoted by the subscript 2, then $x_1 \tilde{y}_2^\beta = \bar{x}_1 \bar{\tilde{y}}_2^\beta$. The case where point 1 is at the nose of the profile and point 2 is at the sonic point on the contour corresponds to that discussed previously for the cusped body.

The flow field in the vicinity and in the interior of closed axisymmetric bodies has been considered previously. Karman (Reference 7)

Correlation of Basic Planar Solutions in the Physical Plane with Holograph Solutions

$f_1' = 4/27 \dots$. Using Equation (4) for x and y:

$$\zeta = (\gamma+1)^{-1/3} x \bar{y}^{-4/5} = \xi = A_{-1} (\gamma+1)^{-1/3} |\eta|^2 (f_{-1} + 3\xi f_1') [-3(\gamma+1)^{-1/3} |\eta|^{-5/2} f_1']^{-1/5}$$

For $\gamma = 1.4$, $A_{-1} = 1.018$. Using this value for A_{-1} gives the same asymptotic values at any point x, y in either system.

Let Equation (16) be applied to the previously discussed cusped body in an \bar{x}, \bar{y} plane such that the length and height to the sonic line are given by $x\bar{s} = 1.0$ and $y\bar{s} = .1736$. This body corresponds to the 20° wedge which was used in the experimental phase.

The flow for such a body can be obtained by choosing A_2/A_{-1} to give the proper thickness ratio and then applying a scale change $\bar{x} = Z_2 x, \bar{y} = Z_2 y$

since $x\bar{s} = A_{-1} (A_2/A_{-1})^{2/3}$ (2.08) and $y\bar{s} = A_{-1} (A_2/A_{-1})^{1/6}$ (2.47)

$$\frac{y\bar{s}}{x\bar{s}} = \frac{\bar{y}\bar{s}}{\bar{x}\bar{s}} = \frac{.1736}{1.0} = \frac{A_2}{A_{-1}} \frac{1/2}{2.08} \quad \text{or} \quad \frac{A_2}{A_{-1}} = 47.0$$

and $Z_2 = .0364$

If a streamline of interest is at $Y = 3.00$, the following relations can be used to get the asymptotic results from the solutions in the physical

plane: $X = Z_2 (\gamma+1)^{1/3} (Y/Z_2)^{4/5} = 1.65 \xi$

$$Y = 5 Z_2 (Y/Z_2)^{1/5} \bar{Y} = .441 \bar{Y}$$

$$C_p = 2(\gamma+1)^{-1/3} (Y/Z_2)^{2/5} f' = .256 f'$$

These results will be used in a later discussion.

The solution given for the basic singularity of axisymmetric flow should at sufficient distances give the correct flow fields for all bodies of finite span. Again the problem is to determine the relation between the "strength" of the basic singularity and the body dimensions. It is of interest to determine whether the "sufficient" distance is a practical one in terms of model and tunnel dimensions.

Lifting Cases

A convenient way to treat bodies at small angles of attack is to linearize the shift of the mapping in the hodograph plane. If we consider the case where the mapping of the body is close to the original one, and

we let $\bar{\eta}(\theta) = \bar{\eta}_0(\theta) + H(\theta)$ be the map of the body in the hodograph, let $\phi(\eta, \theta) = \phi_0 + \Omega$ be the new potential, and further let $f(\theta) = f_0(\theta) + F(\theta)$

be the map of the body in the physical plane, Guderley has shown in

Reference 6 that the new linearized boundary condition is

$$\Omega_{\bar{\eta}} + \bar{\eta}_0 \Omega_{\theta} d\bar{\eta}_0/d\theta = F(\theta) - F(\theta) = 0$$

if the body location or contour in the physical plane does not change.

Cusped Lifting Bodies

The simplest body with lift that can be treated is that given by $n = -1, 1/2$, and 2. If $\phi_0 = A_1 \eta^{-1} f_1 + A_2 \eta^2 f_2 \dots (16)$, $\Omega = A_{1/2} \eta^{1/2} f_{1/2} \dots (17)$

and if the original body is moved through an angle α , while the singularity remains at the origin of the η, θ plane, the boundary condition is given

by $\Omega_{\bar{\eta}} d\theta/d\bar{\eta}_0 + \bar{\eta}_0 \Omega_{\theta} - \alpha = 0$ substituting of (16) and (17) into this expression gives:

$$\alpha = A_{1/2} \zeta^{1/2} f_{1/2}' \left\{ \frac{A_1}{A_2} \left[\zeta - 1 \right] \left[\frac{1}{2} \frac{f_{1/2}'}{f_{1/2}} + 3\zeta \right] \left[\frac{10}{3} \zeta + \frac{2}{9} \frac{f_2'}{f_2} + \frac{2}{9} \frac{f_{-1}'}{f_{-1}} \right] + 3 \right\} \quad (18)$$

It is possible to satisfy this equation at only one point by a choice of $A_{1/2}$.

Reference 1, page 34, gives recurrence relations between f_n and $f_{n+3/2}$ which yield:

$$\begin{aligned} f_{1/2} &= |\zeta|^{1/2} \{ f_{-1} + 2(\zeta - 1) f_{-1}' \} \\ f_{1/2}' &= -\frac{1}{18} |\zeta|^{1/2} f_{-1}' \end{aligned} \quad (19)$$

Using these relations, if $\zeta = 0$ is chosen as the matching point,

$$A_{1/2} = 8\alpha/\sqrt{3} \quad \bar{\gamma}_{1=0} = (\gamma+1)^{1/3} \alpha (9A_{-1}/A_2)^{1/3}$$

The resultant camber shape can be found by an integration of the average values of the slopes of the upper and lower sides of the body, and the numerical results as shown in Figure 4a indicate it to be parabolic. The resultant camber line shape and lift data are shown in Figure 4. This particular case may not be too enlightening, but it can be expected that the chord line could be caused to pass through any desired number of additional points on a straight line by taking higher order terms and properly choosing the coefficients. The resultant body would still have a camber line which is not straight, but the deviations might not be significant in the results. The inadequacy in the nose region also exists in the other approaches to the lifting problem in transonic flow presently in use.

In regard to the effect on the walls of a tunnel on lift of such bodies, since the predominant lifting term will be given by $\phi_{1/2}$ and $A_{1/2}$ will be proportional to α , for $\alpha \ll \theta_0$ it is apparent that the lifting effect will be of lower order than the basic singularity. This is in contrast to the subsonic cases where the influence of lift predominates over the influence of thickness at far distances.

Wedge Profile with Lift

In Reference 5, the method of linearizing the boundary condition is used to find the change in flow due to angle of attack on the previously determined flow of a double wedge airfoil. In this case the $F(\theta) = 0$, i.e., the wind direction is changed but not the body attitude. The singular point then moves from the origin of the η, θ plane to a point $\eta = 0, \theta = \alpha$. The boundary conditions are then satisfied along the lines $\theta = \pm \theta_0$ and also along the characteristics emanating from $\eta = 0, \theta = \pm \theta_0$. It is shown that for sufficiently small angles of attack, the "separation bubble" which must occur at the nose has negligible influence on the lift.

The resultant change in pressure distribution based on the assumptions mentioned is shown in Figure 2c.

With these results, one is led to reason that a "transonic dip" may exist in the $dC_L/d\alpha$ curve for wedges with thickness ratios greater than about .10. Results have previously been obtained analytically for the incompressible lift of a double wedge. When a Prandtl-Glauert correction is applied, this gives for all subsonic Mach numbers higher values of $dC_L/d\alpha$ than those obtained at Mach One. (The accuracy of these results is open to question because of the infinite velocities which arise at the shoulder and at the nose). The values obtained for purely supersonic

flows are also higher. The Mach One results further indicate a horizontal tangent to this curve. Hence, it would appear as though the curve has a rather unusual behavior without considerations of viscosity. This is one of the problems which would seem to justify considerable effort in obtaining experimental data at Mach numbers very close to one.

In most practical problems with three dimensional bodies it would be difficult to find the relation between the basic singularity and the body dimensions analytically. In light of this, an experimental program has been initiated to help fix the body shape parameters which would effect the flow field configurations at large distances.

SECTION II

PRELIMINARY EXPERIMENTAL STUDY

One of the more obvious ways of simulating a free streamline in a wind tunnel is to have flexible walls which can readily be adjusted to a desired set of ordinates. The 6" supersonic tunnel at WADC is awaiting delivery on such a piece of equipment, and in preparation for a program utilizing this device, some preliminary work has been done with a set of fixed geometry blocks which have a throat followed by a long, straight section. See Figure 5b.

The initial purpose for conducting this preliminary study was to obtain some idea of the influence of the tunnel boundary layer under the pressure rise which exists ahead of a model in Mach One flow. Because of this, a comparatively large model was used. It was also desirable to determine whether or not it was possible to simulate planar flow by shaping the portions of the model near the walls so that the boundary layer on the wall would not change the effective thickness of the model in that region.

It will be noted in Figure 3a that the free streamline have inflection points quite close to $X = 0$. Consequently, one might obtain a fairly good approximation of the desired flow field if the correct slope is simulated by the straight wall at the model abscissa. It is necessary, however, to evaluate the effect of small changes in wall contour on the flow in the vicinity of a model.

It is also of interest to determine how much relatively large changes in wall configuration will effect the flow in the vicinity of a given body. It can be seen that if the divergent walls which were used in this study were made effectively parallel, the result would be a "choked" flow. This corresponds approximately to a free flow at some Mach number which is higher than the upstream Mach number in the choked tunnel but less than one. It is further evident from continuity considerations that with parallel walls and a symmetrical pattern, on isobar corresponding to the upstream pressure would divide those other isobars which went from the wall to the model and those which crossed the tunnel centerline.

One can expect, in this case, that if the pressure drops continuously on a model toward the rear, a monotonically increasing Mach number at least to the sonic line along the wall of such a tunnel will exist.

A further question of importance involves the effect of lifting bodies on the flow patterns. In this preliminary phase, the wall and model pressure distribution were obtained for a 20° wedge at angles of attack up to 6° .

Experimental Equipment

1. Wind Tunnel

This tunnel was a 6" square test section and is powered by an Allis Chalmers 1000 hp axial flow compressor. The vertical walls of the test section are glass panelled. The nozzle blocks are equipped with static pressure orifices. The block ordinates are shown in Figure 5b. Both mercury and TBE manometer panels are provided for obtaining pressure data.

2. Optical Equipment

The system for flow visualization includes interferometer, schlieren, and shadowgraph with arrangements for photographing with Polaroid Land film or conventional film. A comparison of interferograms with pressure data indicates that at the density level used, the inherent inaccuracy of this interferometer is about ± 0.02 in Mach number and consequently it was used only to study the flow pattern qualitatively in this program. Some of the resultant interferograms and schlieren photographs are shown in Figures 8, 9 and 12.

3. Wedge Model (See Figure 10)

A 10° half angle single wedge of 1" chord and $5 \frac{1}{4}$ " span was used in the preliminary runs. In an attempt to simulate planar conditions as well as possible, the $\frac{3}{8}$ " gap to the glass windows was filled with a plastic material that could readily be shaped. Pressure taps were located at mid-chord at positions $\frac{1}{2}$ " from each tip and also at mid-span in $\frac{1}{8}$ " intervals chordwise. The assembly was mounted to a rod, which could be traversed in the streamwise direction. The shape of the plastic fillers which gave the most nearly planar flow is that shown in Figure 10. It is clear that perfect simulation of planar flow cannot be obtained in this manner. However, the difference in C_p between the tip orifices and the mid-span orifices never exceeded 0.02 during runs where data is taken.

No after body was placed behind the wedge section since it was desirable to minimize any influence of viscosity. Angles of attack were obtained by placing shims above and below the holding screws behind the wedge shoulder.

4. Biconvex Model (See Figure 12)

A biconvex section with the same chord and thickness as the wedge was also fabricated. This had two orifices placed at the mid-chord, mid-span position, one on top and the other on the bottom. The same plastic spacer was used for tests with this model.

Wind Tunnel Runs

All runs were made with $P_0 = 1000$ PSF and $T_0 = 100^\circ\text{F}$. Pressure data were taken from a TBE manometer. The following is a listing of the configurations of the runs which were made in this phase:

| <u>Model</u> | <u>in Degrees</u> | <u>Nose Station</u> | <u>Run No.</u> |
|--------------|-------------------|---------------------|----------------|
| Wedge | 0 | 42" to 58" | 0 to 32 |
| Wedge | 2, 4, 6 | 42" to 58" | 33 to 82 |
| Wedge | 1/2, 1, 1 1/2 | 45" | 83 to 89 |
| Biconvex | 0 | 42" to 58" | 90 to 95 |
| Biconvex | 1/2, 1, 2 | 46" | 96 to 100 |
| Biconvex | 2 | 42" to 58" | 101 to 112 |

Discussion of Experimental Results

The two initial problems of the preliminary phase do not seem to have any troublesome consequences. It is not likely that separation or appreciable boundary layer thickening will occur at the walls of a flexible nozzle in the regions of interest even with comparatively large models. For the configurations which will be used for the next phase, the simulation of planar flow by shaping the plastic fillers at the tips is quite satisfactory.

The aerodynamic data obtained appear to be quite interesting. Figure 6a shows the wall pressures which were obtained by traversing the wedge model from Station 42 to Station 56 at $\alpha = 0$ while Figure 9a shows the corresponding schlieren pictures. With the model in the most downstream position, the flow is choked by the model support system. This can be seen from the fact that forward movement of the model does not influence the shock position. There is a supersonic region downstream of the throat which is terminated by a normal shock. The flow pattern ahead of the model as shown in the schlieren is at some subsonic velocity ($M = .75$) where the local supersonic region first begins to grow at the shoulder of the wedge. The first "choking" by the model is evidenced by the forward movement of the tunnel shock, and also by the appearance of sonic pressures at the wall. As the model is moved forward the supersonic region grows until it fills the entire rearward field of view.

It will be noted that the pressure distribution at the wall approaches the theoretical form for Mach One as the wedge is moved forward. At Station 46 for $\alpha = 0$ the wedge pressures (Figure 5a) as well as the wall pressures (Figure 5c) are very close to the values given by similarity theory.

For the additional tests that were run, this position was considered to be the optimum configuration which could be obtained with these nozzle blocks. It can be seen that if a Mach One flow can be sufficiently well simulated at a model by these straight blocks, it corresponds to a free flow over that model with some other body or "source distribution" far out in the flow field. If another model of the same basic singularity strength is substituted for the original one, the resultant pressure distribution at the wall due to this basic singularity should not change. Hence, it might be possible to find the body shape parameters without an ideal wall shape. The results obtained thus far have been quite encouraging.

In Figure 5c the dotted line shows the pressure distribution given by the basic singularity, and the dashed line is the distribution given by a cusped body of the same length and thickness to the sonic line as the wedge which was used. Based on the foregoing discussion of the analytical results, the theoretical pressure for the wedge itself should be very close to this.

The pressures on the surface of the wedge at Station 46 are in very good agreement with the theoretical values of Reference 3 for at least 80% of the surface. The nose region is not accurately described by Reference since the $|\eta|$ goes to infinity under the approximations used while the actual flow should have a stagnation point at the nose. Dr. Guderley has recently corrected these results to include the nose region.* The corrected pressure distribution is also shown in Figure 2b. The agreement with the uncorrected theory is apparently a compensation of the approximation errors of the theory and the thickening effect of the boundary layer.

Wedge at Angle of Attack

Figure 7b shows the lift data obtained by recording the pressures on the surface of the wedge for α from 0 to 6° . Since only one side of the wedge had enough holes to obtain the pressure distribution, runs were actually made with corresponding positive and negative angles of attack. To check whether the angles were the same, the orifices at the mid-chord point of the opposite side were also recorded, and it was necessary that the pressure at this point match the curve for the corresponding run.

It will be noted that there are two distinct regions of this lift curve. The dashed line is the theoretical value obtained in Reference 5 for $\alpha \ll \theta_0$. It can be expected that as the supersonic region at the nose grows, the actual curve will deviate from the one obtained analytically

*Report to be published.

by neglecting this region. When the entire upper side becomes supersonic the body can be expected to act essentially like a flat plate. The flat plate follows the relation $C_L \sim \alpha^{2/3}$, and hence, the steeper slope. For thinner wedges the range of angles of attack where is less and consequently the transition will occur sooner.

Biconvex Section

Figure 11 shows the wall pressure data obtained with the model nose at Station 46. This appears to have the closest to correct pressure pattern. Comparison of this pattern with that given by the wedge reveals some interesting information. The maximum C_p for the biconvex section is .300 while for the wedge it is .334. From the similarity considerations previously discussed, for the wedge the scale factor Z_2 is .0364. If it is assumed that the ratio of the values of C_p would be the same asymptotically since $C_p = 2(K+1)^{-1/3} f'(\frac{Y}{Z_2})^{-2/5}$, for the biconvex section, the value of Z_2 would be .0264. The interferogram for this run (Figure 12) indicates that the sonic line is at $X_5 = .400$. The "corresponding" cusped body or wedge of this length to the sonic line has a height to that $Y_5 = .113$. The geometry of the biconvex section gives $Y_5 = .113$.

Hence, there is agreement in the role of Y_5^4/X_5 for all three sections thus far considered.

Conclusions

A. The analytical results indicate:

1. Within the accuracy of the numerical methods used, wedges and cusped bodies of the same length from the nose to the sonic line and thickness at the sonic line give the same asymptotic flow fields.
2. Planar bodies of a given family which give the same asymptotic flow fields have the same values of Y_5^4/X_5 . This value is proportional to A_3^{-1} .
3. For planar flows, over bodies of normal thickness ratios, the distance, where the streamline shape will be given sufficiently well by the "basic" solution, is within the bounds of experimental feasibility. In the example considered it is about 20 chord lengths.
4. For moderate angles of attack the influence of lift on wall configurations is small compared to the influence of thickness.
5. For the axisymmetric case, asymptotic solutions are also given, but it is not clear how to correlate these results with particular closed body shapes except by experiment.

B. The Preliminary Experimental Study Indicates:

1. Even for the ratios of tunnel height to model thickness less than twenty, which were used in this study, good agreement with theoretical results at Mach One can be obtained.

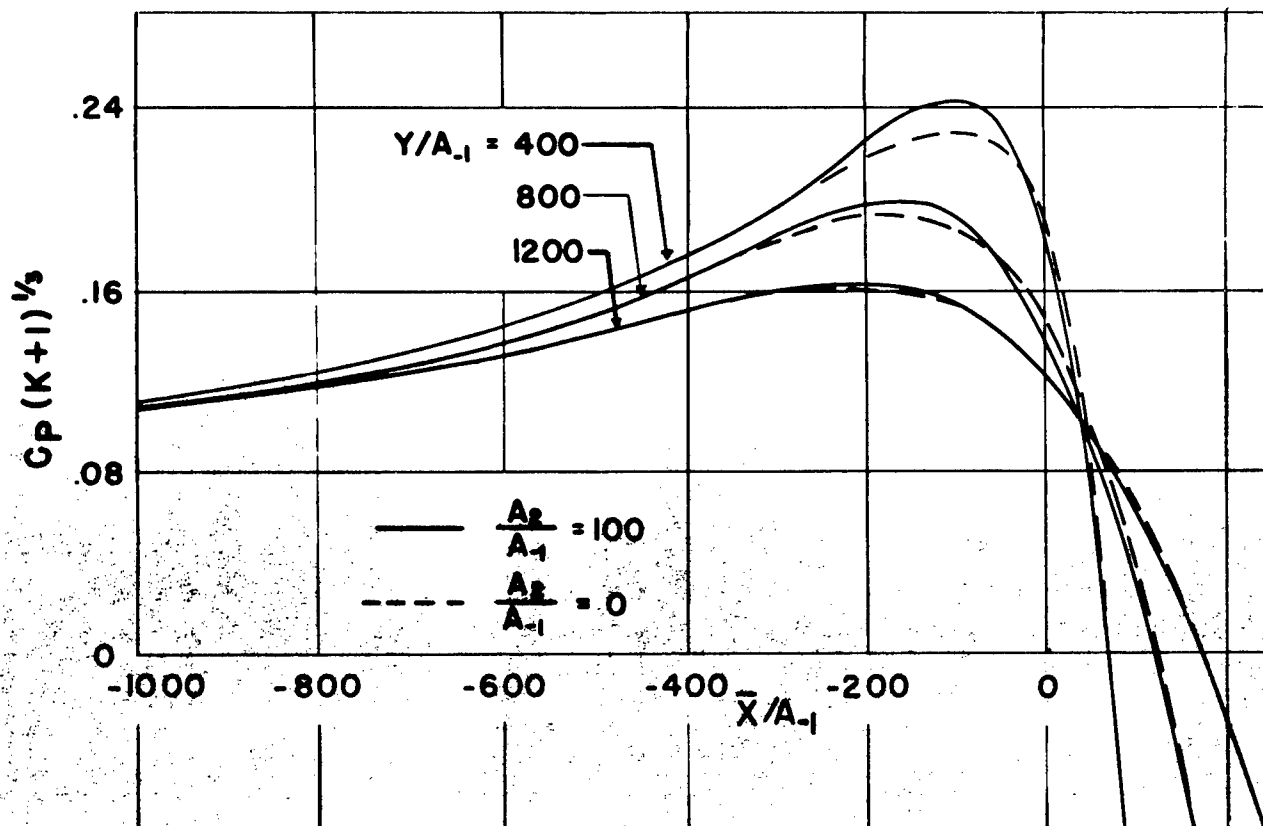
2. The straight walled tunnel appears worthy of further study as a means of simulating sonic planar flow over bodies.

3. With due consideration for the crudeness of the experimental setup, pressure distributions on a wedge with $\alpha \ll \theta_0$ are in good agreement with the predictions of Reference 3 and 5.

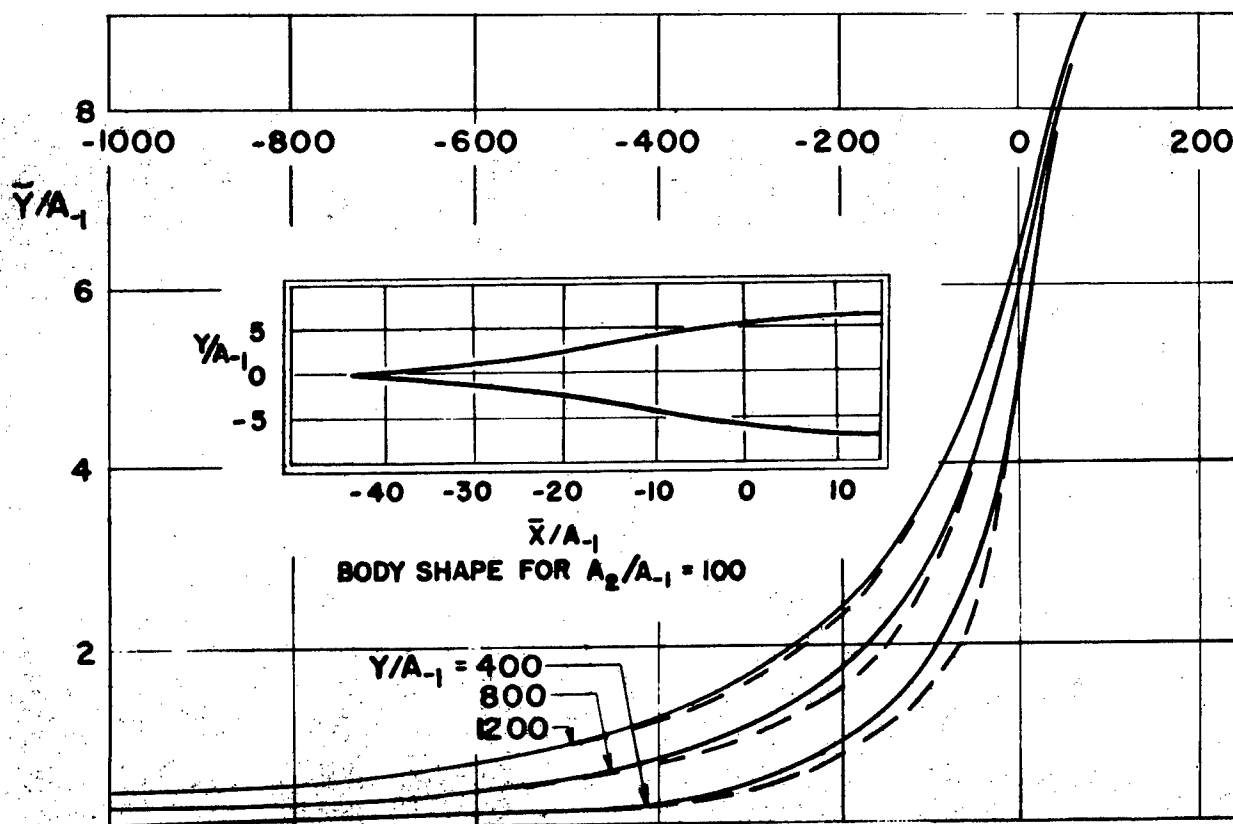
4. There is evidence that the value of $\gamma \delta^4 / \kappa \delta$ is the parameter which will determine the basic source strength and hence, the wall configuration.

REFERENCES

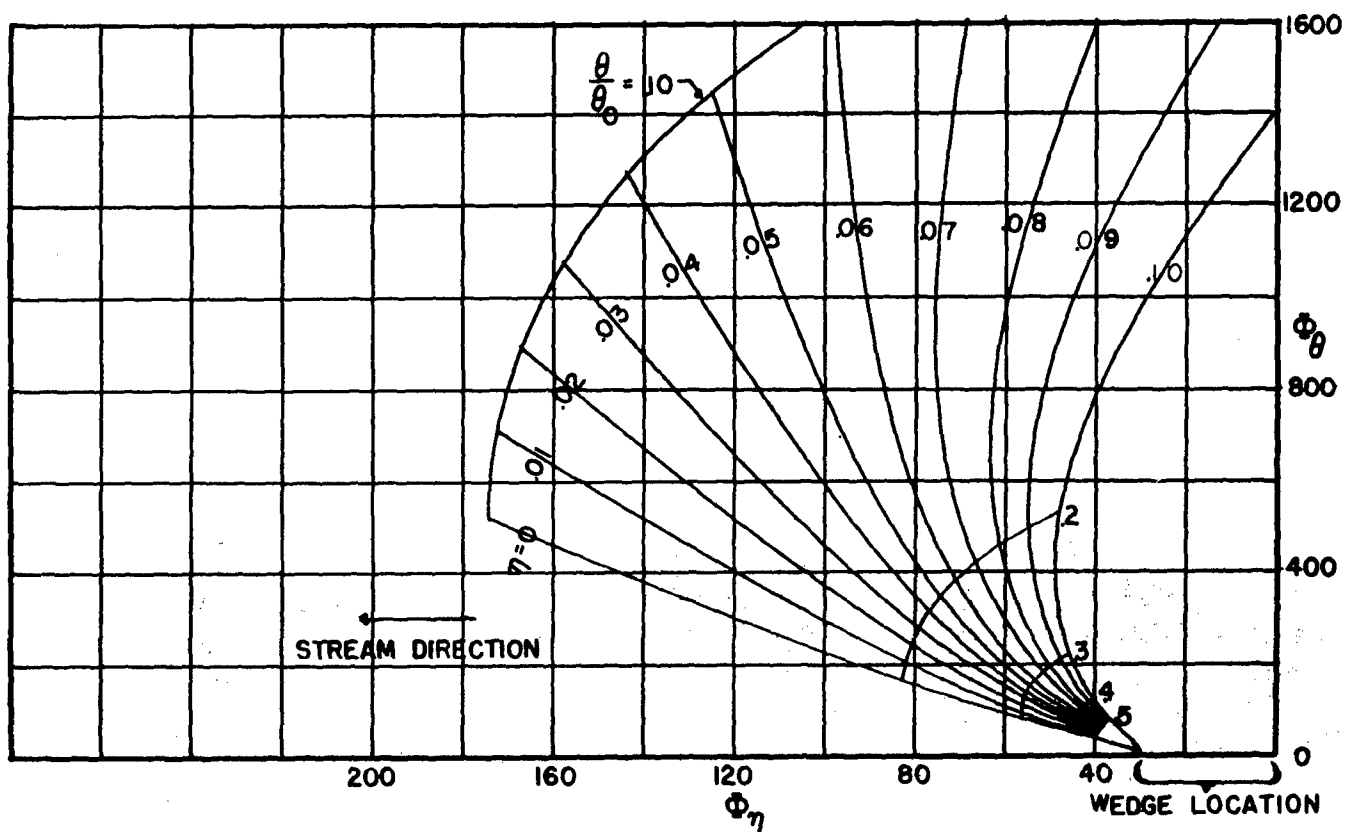
1. Guderley, K. G. Singularities at the Sonic Velocity. USAF Technical Report No. F-TR-1171-ND. 1948. (Unclassified, English)
2. Guderley, K. G. and Yoshihara, H. Flow over A Wedge Profile at Mach Number One. USAF Technical Report No. 5738, 1948. (Unclassified, English)
3. Guderley, K. G. and Yoshihara, H. Axial-Symmetric Transonic Flow Patterns. USAF Technical Report No. 5797, September 1949. (Unclassified, English)
4. Barish, D. T. and Guderley, K. G. Asymptotic Forms of Shock Waves in Flows over Symmetrical Bodies at Mach One. USAF Technical Report No. 6660, March 1952. (Unclassified, English)
5. Guderley, K. G. and Yoshihara, H. Two Dimensional Unsymmetric Flow Patterns at Mach Number One. USAF Technical Report No. 6683, January 1952. (Unclassified, English)
6. Guderley, K. G. Two Dimensional Flow Patterns with A Free Stream Mach Number Close to One. USAF Technical Report No. 6343, May 1951. (Unclassified, English)
7. Karman, Theodore von. The Similarity Law of Transonic Flow Patterns. Journal of Mathematics and Physics. October 1947. Volume 26, pp. 182-190. (Unclassified, English)
8. Perl, W. and Klein, H. M. Theoretical Investigations of Transonic Similarity for Bodies of Revolution. NACA Technical Note No. 2839, December 1950. (Unclassified, English)



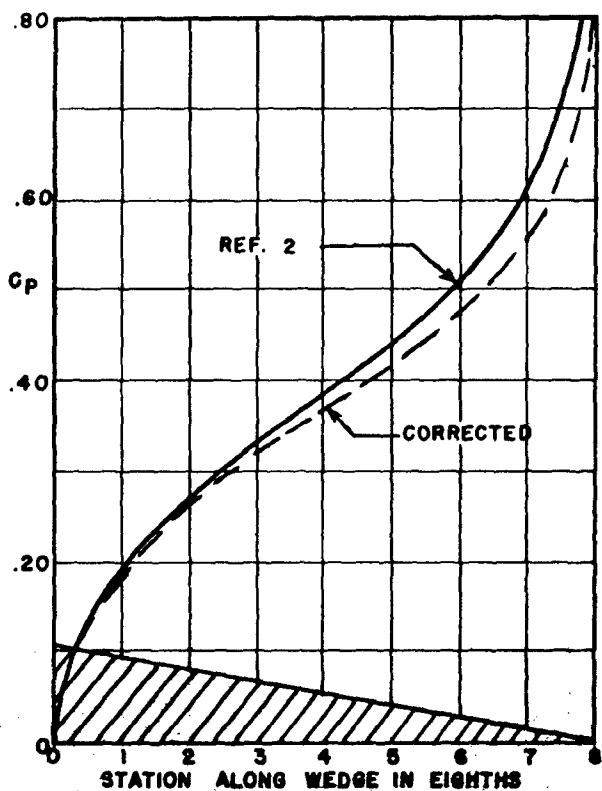
a. PRESSURE DISTRIBUTION ALONG LINES OF CONSTANT Y/A_{-1}



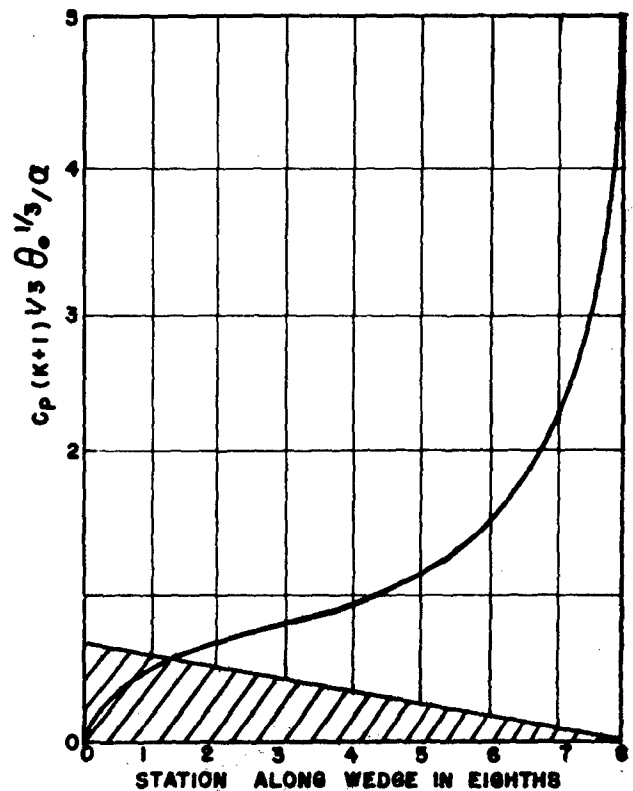
b. DEVIATIONAL ORDINATES OF STREAMLINES
THEORETICAL DATA FOR CUSPED BODY



a. SUBSONIC PORTION OF FLOW FIELD ABOVE WEDGE ($\theta_0 = 10^\circ$)

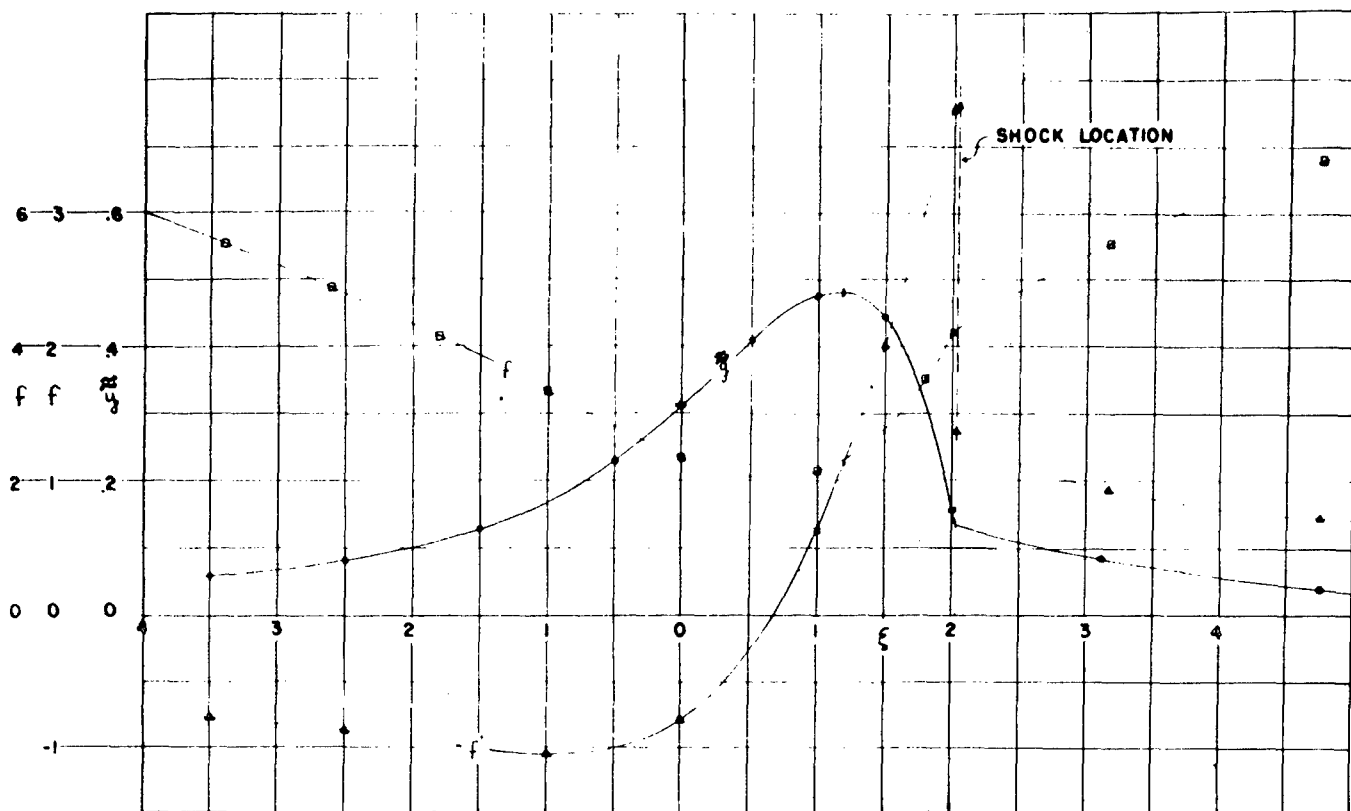


b. PRESSURE DISTRIBUTION ($\alpha=0, \gamma=1.4$)
 $\theta_0 = 10^\circ$

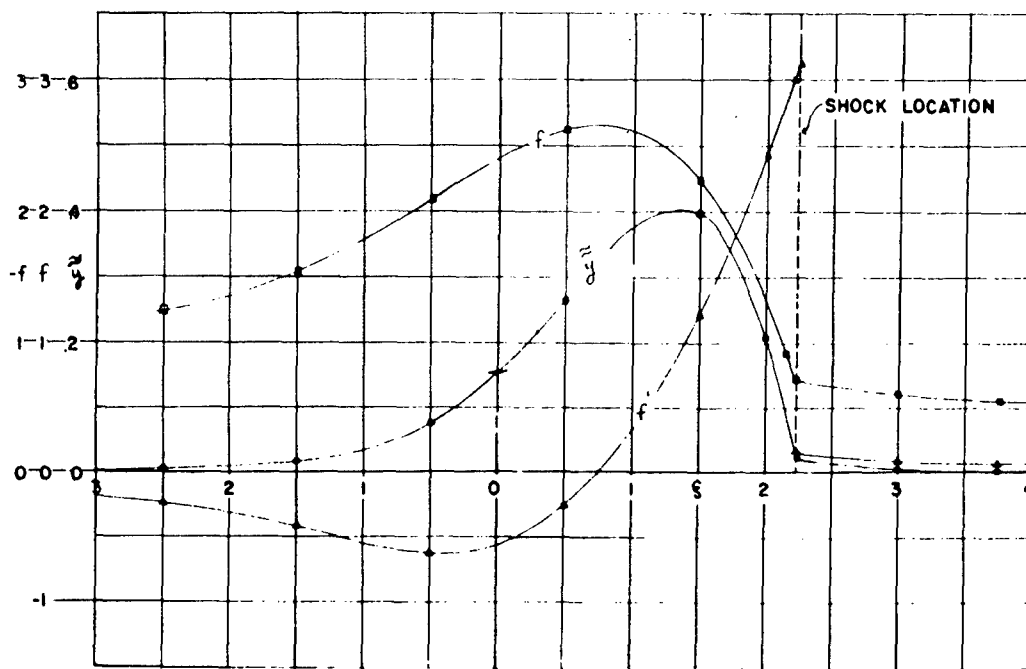


c. CHANGE IN PRESSURE DISTRIBUTION
DUE TO ANGLE OF ATTACK FOR EACH SIDE

FIGURE 2: THEORETICAL DATA FOR WEDGE PROFILES

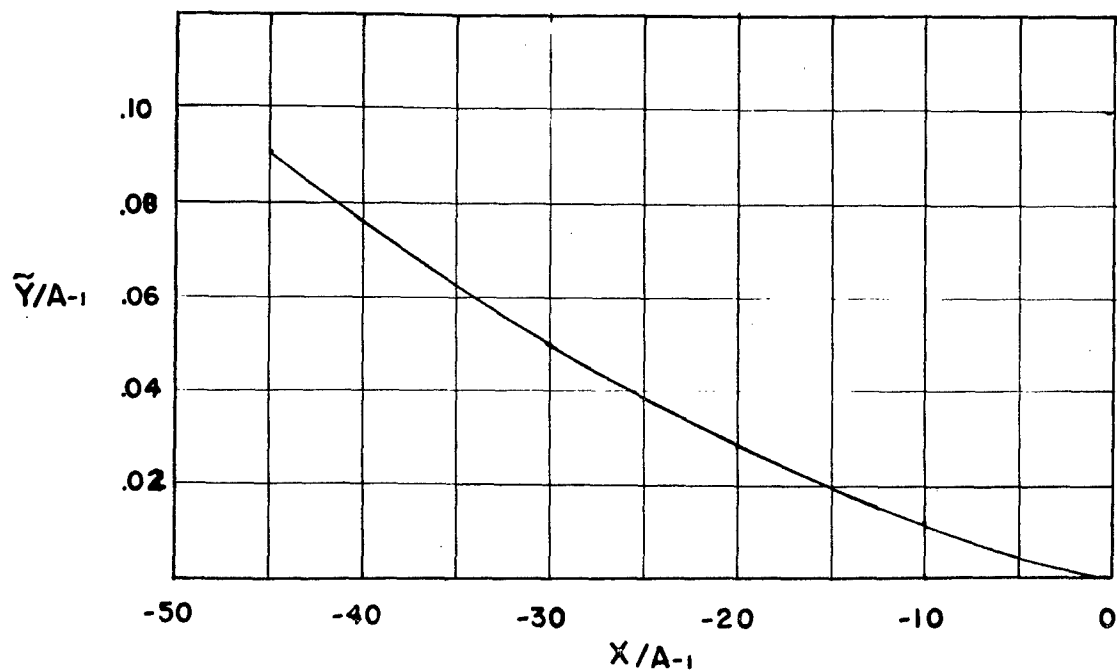


a. FUNCTIONS FOR PLANE FLOW

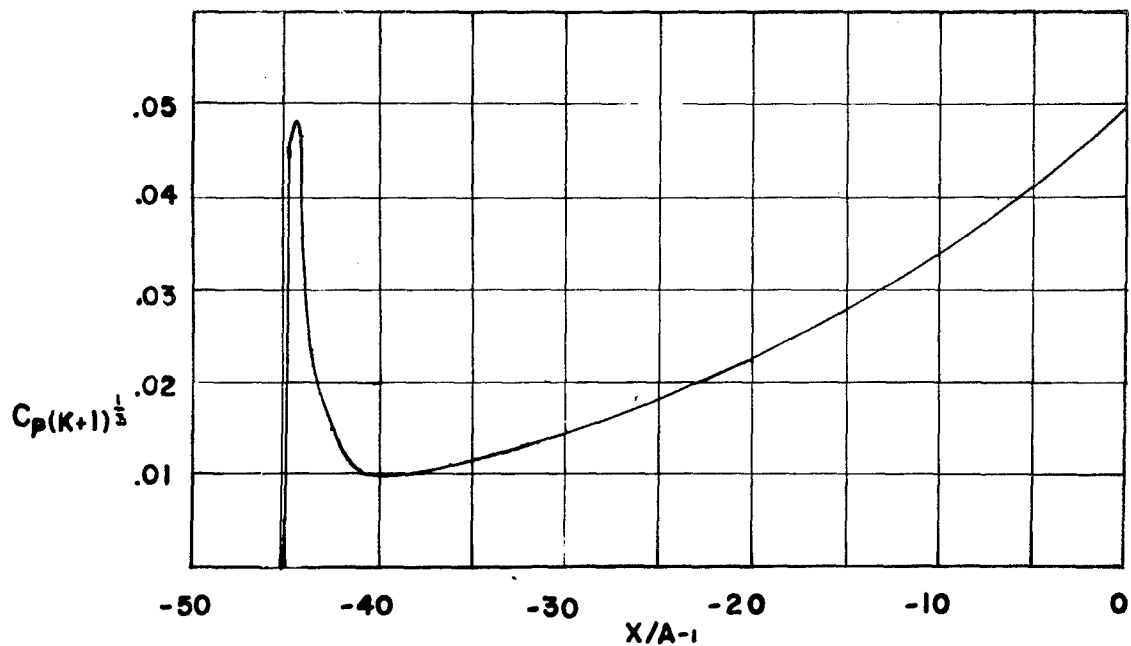


b. FUNCTIONS FOR AXISYMMETRIC FLOW

FIGURE 3: ASYMPTOTIC SOLUTIONS IN THE PHYSICAL PLANE

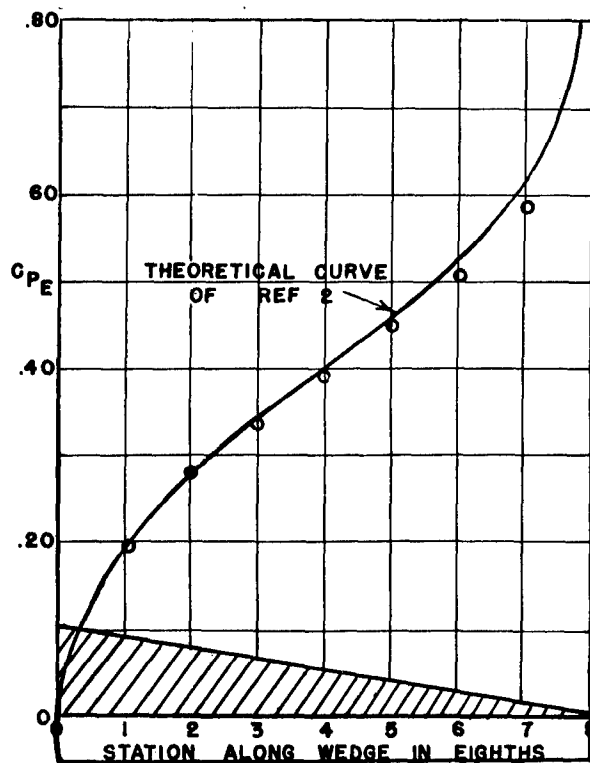


a. CONTOUR OF CAMBER LINE

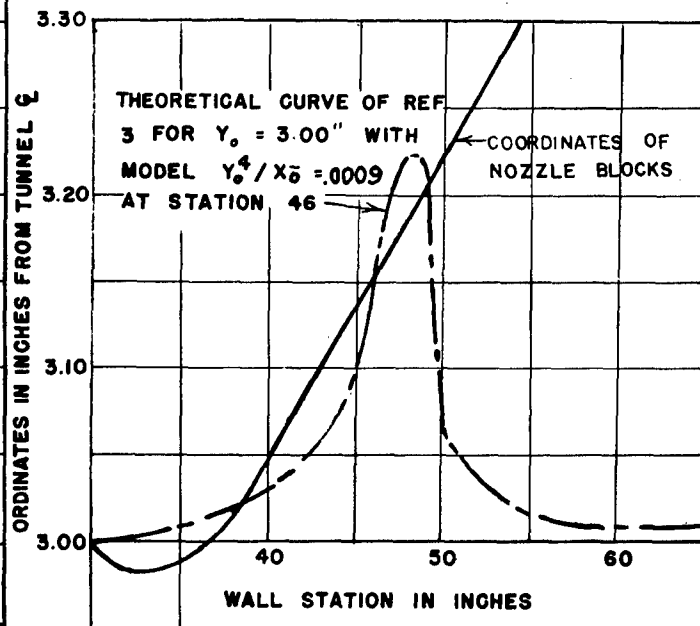


b. LIFT CONTRIBUTION FOR EACH SIDE OF BODY

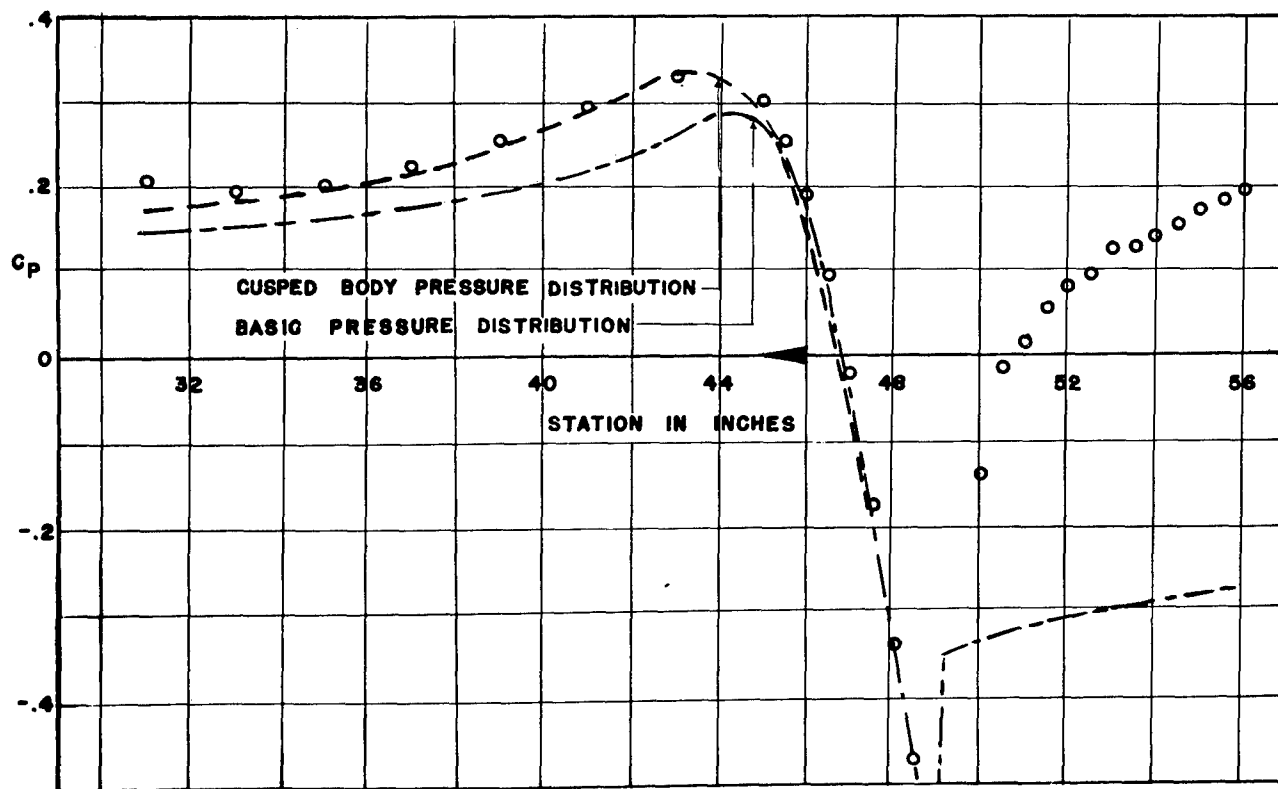
FIGURE 4: THEORETICAL DATA FOR CUSPED BODY WITH LIFT
 $A_2/A_{-1} = 100$ $A/A_{-1} = 2 \quad / \quad 3$



a. PRESSURE DISTRIBUTION



b. WALL CONFIGURATION



c. WALL PRESSURE DISTRIBUTION

FIGURE 5: COMPARISON OF EXPERIMENTAL AND THEORETICAL DATA FOR WEDGE FOR WEDGE AT STATION 46 ($\alpha = 0$)

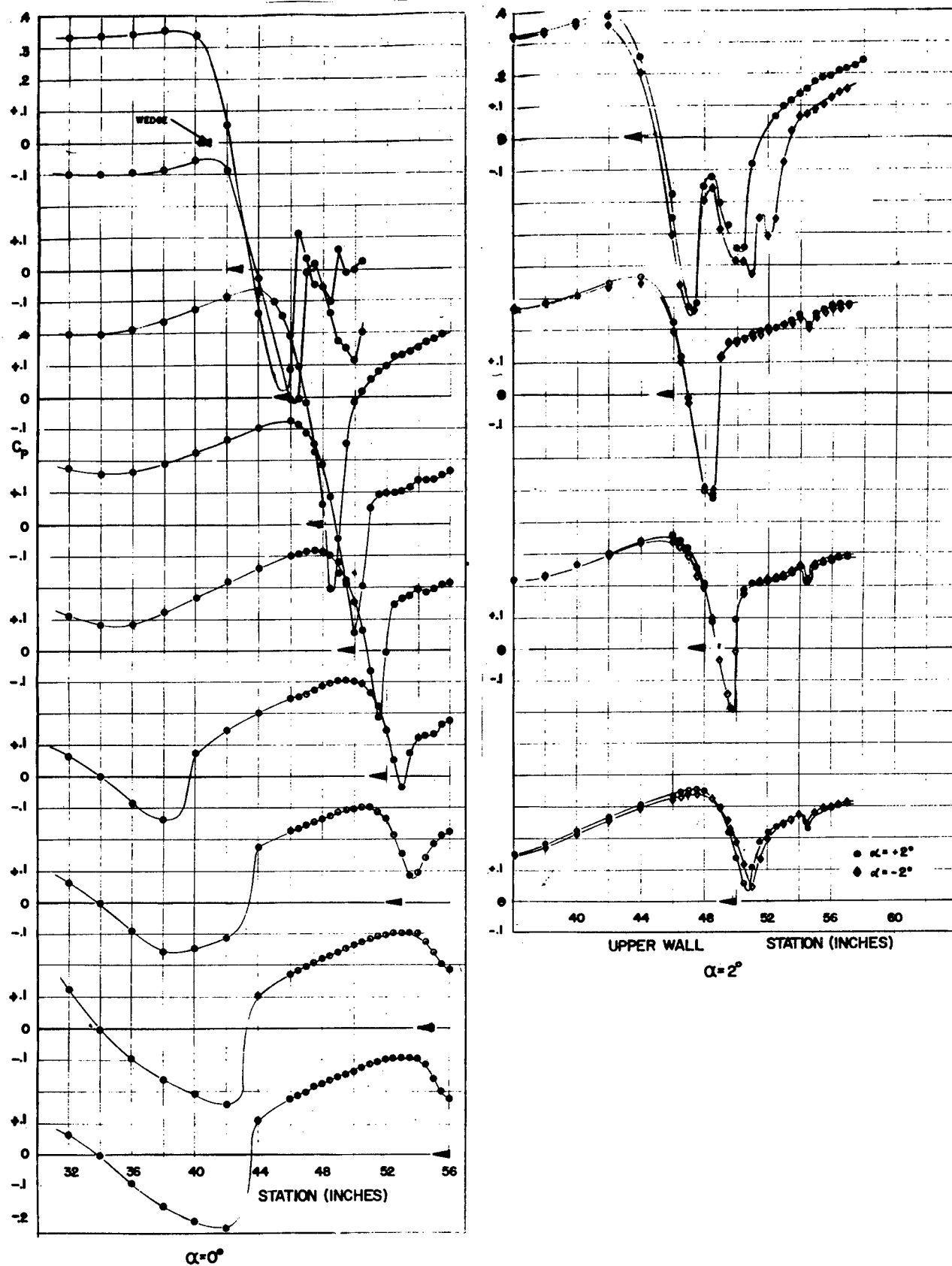
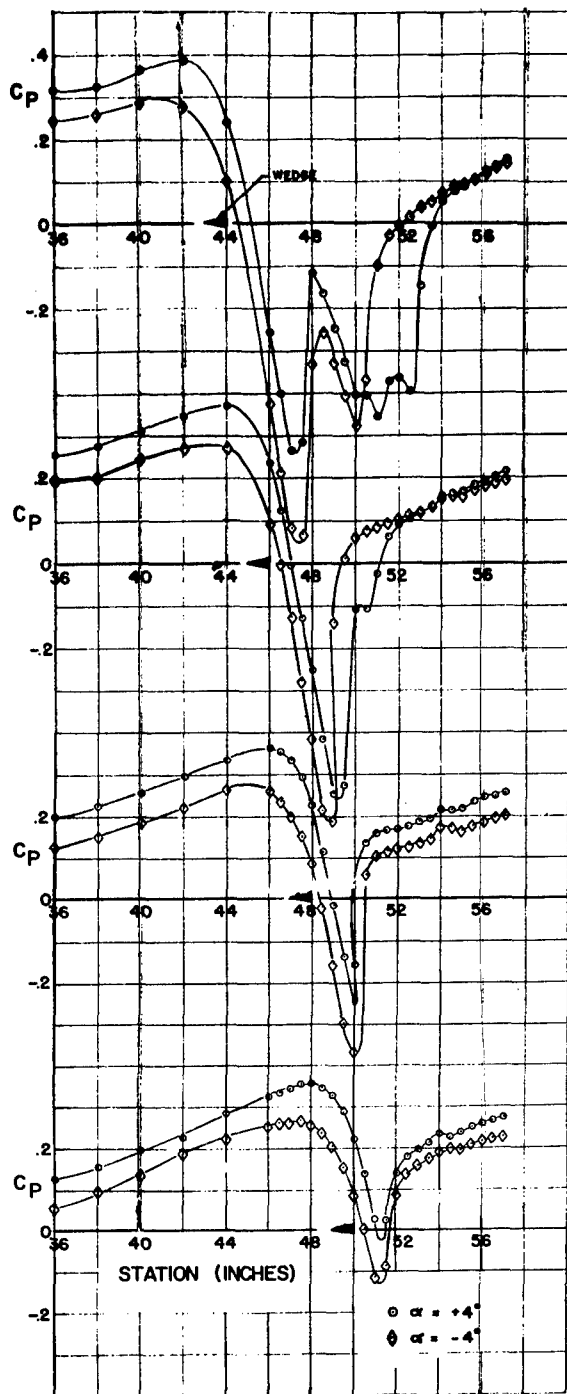
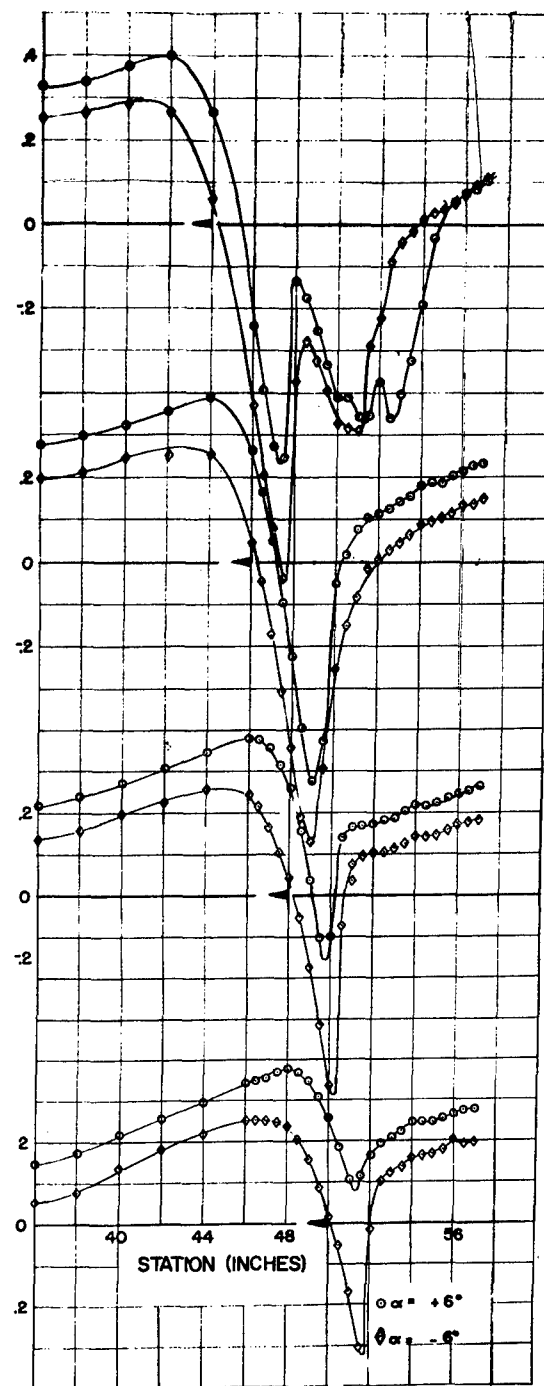


FIGURE 6: EXPERIMENTAL WALL PRESSURE DISTRIBUTIONS FOR TRAVERSES OF 20° WEDGE

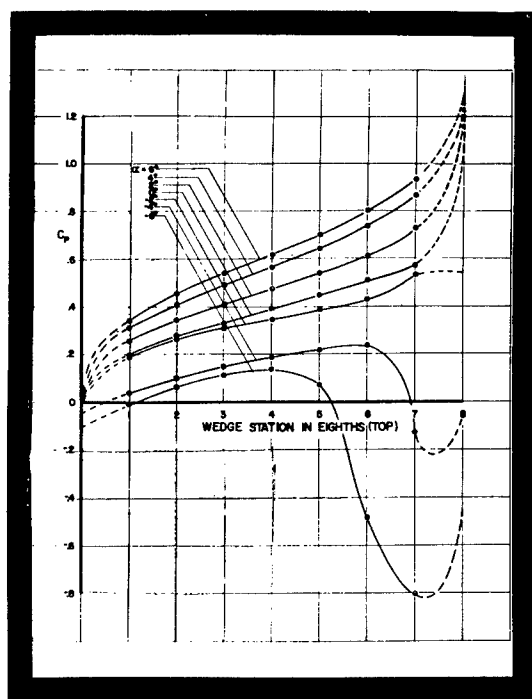


c.

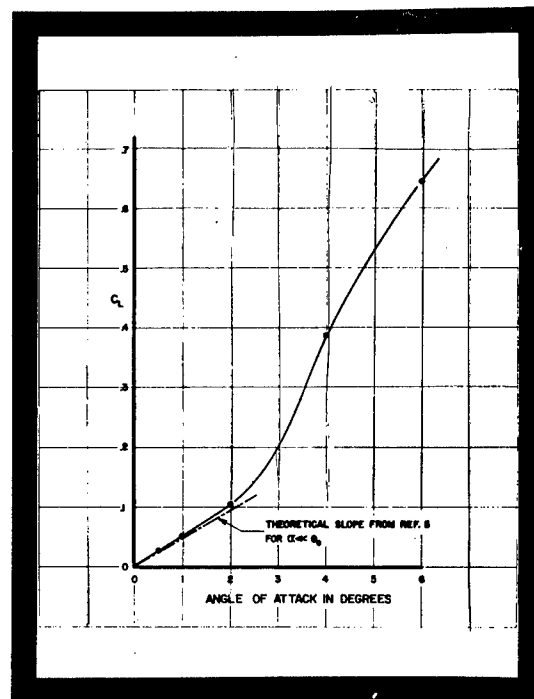


d.

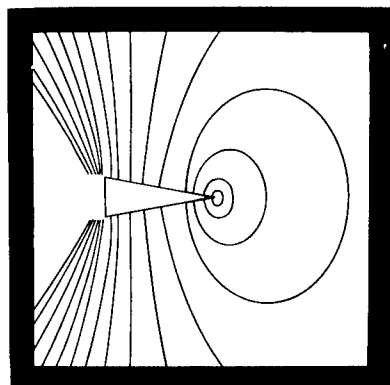
FIGURE 7: EXPERIMENTAL WALL PRESSURES FOR 20° WEDGE WITH LIFT (UPPER WALL)



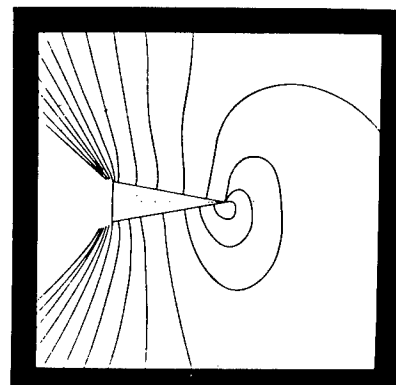
a. DISTRIBUTION IN PRESSURE COEFFICIENT



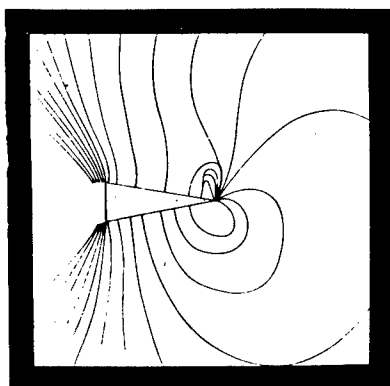
b. LIFT POLAR



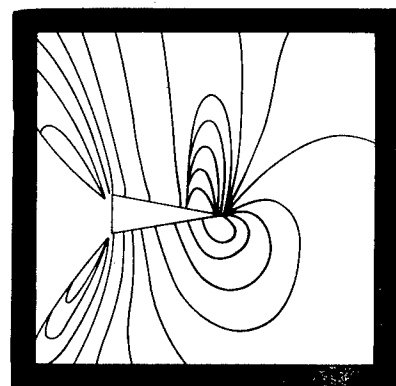
$\alpha = 0^\circ$



$\alpha = 2^\circ$



$\alpha = 4^\circ$



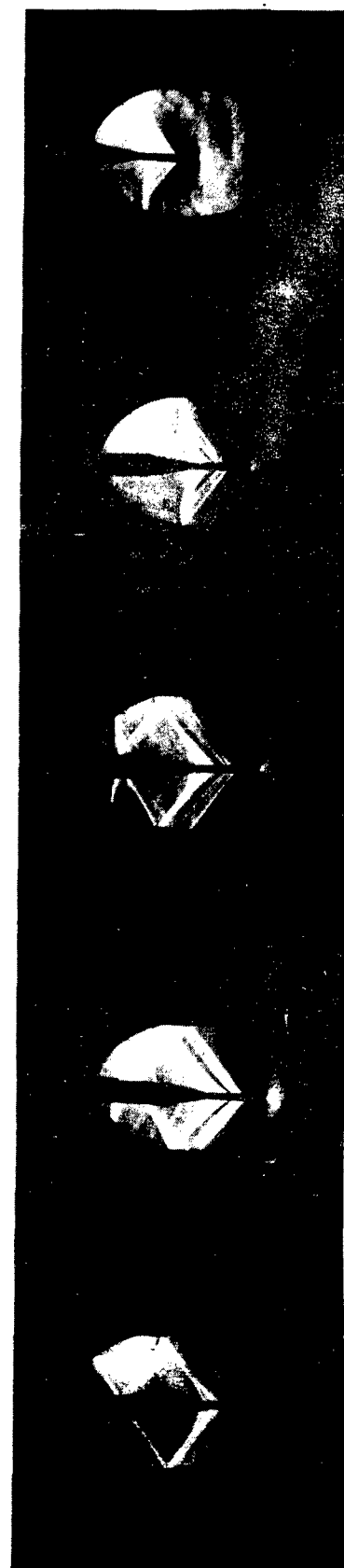
$\alpha = 6^\circ$

c. INTERFEROGRAMS

FIGURE 8: EXPERIMENTAL DATA FOR 20° WEDGE AT STATION 46



20° WEDGE



BICONVEX

FIGURE 9: SCHLIEREN PHOTOGRAPHS OF MODEL TRAVERSES

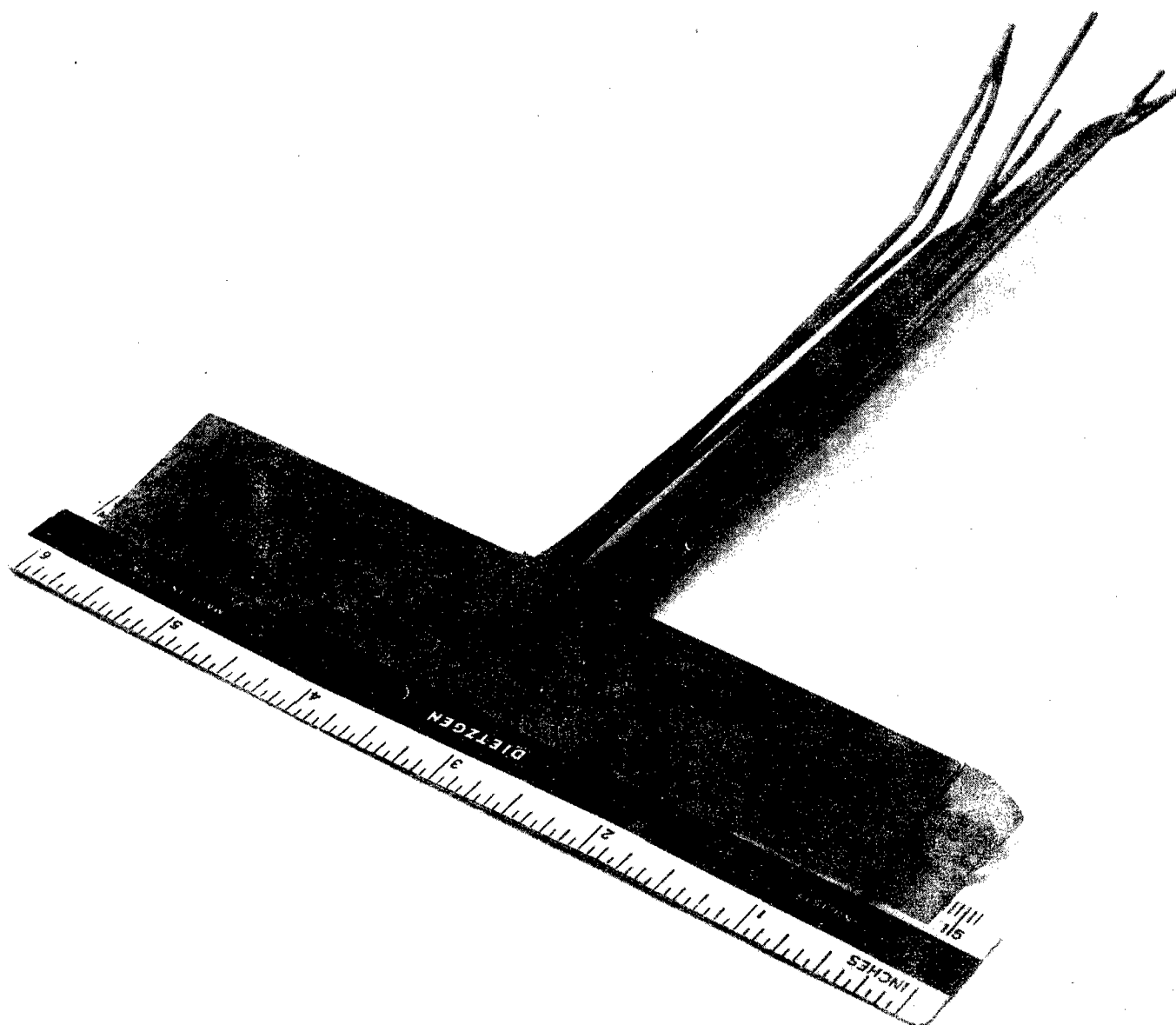


FIGURE 10: WEDGE MODEL

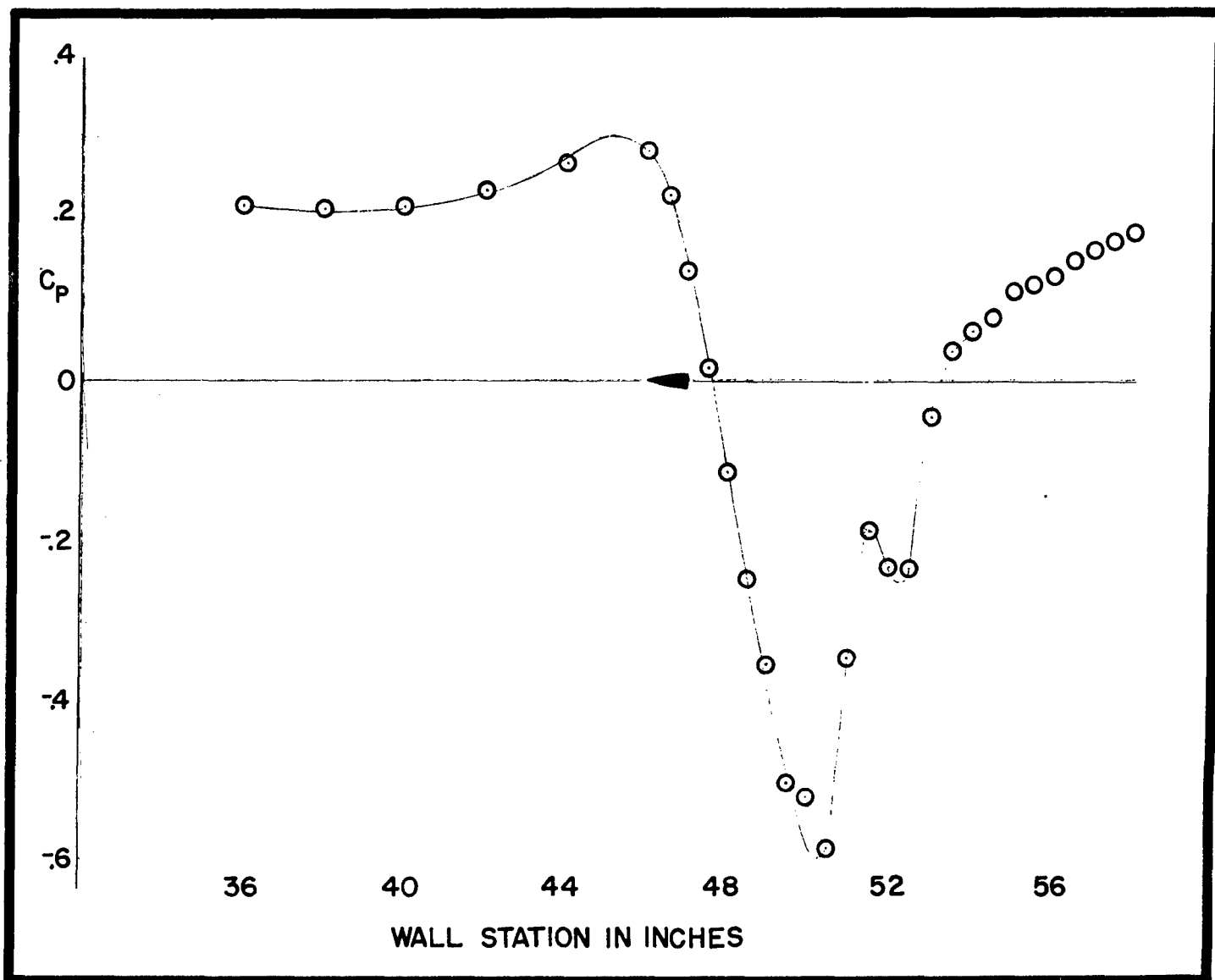


FIGURE 11: EXPERIMENTAL PRESSURE DISTRIBUTION FOR BICONVEX SECTION

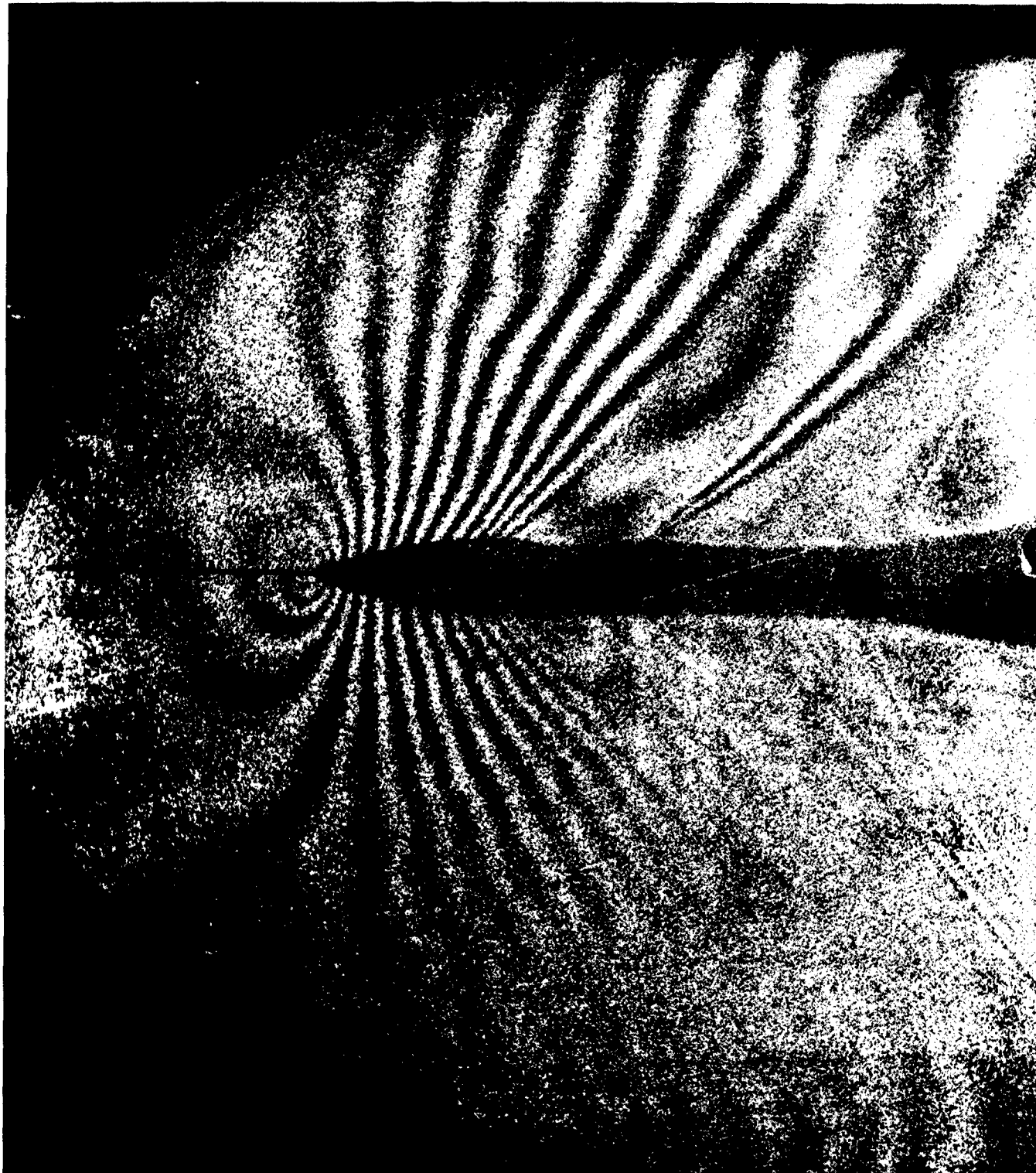


FIGURE 12: INTERFEROGRAM OF BICONVEX MODEL